Atmos. Meas. Tech. Discuss., https://doi.org/10.5194/amt-2017-314
Manuscript under review for journal Atmos. Meas. Tech.
Discussion started: 4 October 2017

Atmospheric Measurement Techniques Discussions

Information content of OCO-2 oxygen A-band channels for retrieving marine liquid cloud properties

Mark Richardson[1], Graeme L. Stephens[1,2]

[1]Jet Propulsion Laboratory, California Institute of Technology, Pasadena, CA 91125, U.S.A.
[2]Department of Meteorology, University of Reading, Reading, RG6 6BB, U.K.

Correspondence to: Mark Richardson (markr@jpl.nasa.gov)

Abstract. An information content analysis is used to select channels for a marine liquid cloud retrieval using the high-spectral-resolution oxygen A-band instrument on NASA's Orbiting Carbon Observatory-2 (OCO-2). Desired retrieval properties are cloud optical depth, cloud pressure thickness and cloud-top pressure and the optimal channels depend on the atmospheric state, cloud properties and position within the OCO-2 swath. Based on information content criteria we select a micro-window of 75 of the 853 functioning OCO-2 channels spanning 763.5—764.6 nm and perform a series of synthetic retrievals with perturbed initial conditions. We estimate posterior errors from the sample standard deviations and obtain ±0.75 in optical depth, ±12.9 hPa in both cloud-top pressure and cloud pressure thickness, although removing the 10 % of samples with the highest χ^2 reduces posterior error in cloud-top pressure to ±2.9 hPa and cloud pressure thickness to ±2.5 hPa. The application of this retrieval to real OCO-2 measurements is briefly discussed, along with limitations and the greatest caution is urged regarding the assumption of a single homogeneous cloud layer, which is often, but not always, a reasonable approximation for marine boundary layer clouds.

1 Introduction

The oxygen A-band spans wavelengths with a wide range of absorption strength and with sufficient spectral resolution these absorption differences can be exploited to determine photon path lengths and therefore retrieve the altitude of cloud tops and the within-cloud photon path, which is related to droplet number concentration and therefore cloud thickness. Meanwhile, continuum reflectance allows a retrieval of cloud optical depth (Fischer and Grassl, 1991a; Koelemeijer et al., 2001; Stephens and Heidinger, 2000). Such a retrieval would allow evaluation of model cloud physics (Bennartz, 2007) and in addition A-band retrievals use reflected sunlight so are physically independent from other common sources of cloud information such as longer wavelength infrared, which may mis-identify cloud-top pressure in the presence of temperature inversions (Baum et al., 2012).

The Orbiting Carbon Observatory-2 (OCO-2) has high spectral resolution so was selected by (Richardson et al., 2017) for a simple cloud-property retrieval with a model-derived lookup table. This combined 20 of OCO-2's 853 functioning channels into 2 "super-pixels" based on their O_2 absorption. The lookup tables were used for all locations and weather conditions and

were validated using collocated MODIS and CALIPSO data (Taylor et al., 2016). Here we develop an optimal-estimation-based retrieval (Rodgers, 2000) for single-layer water clouds over oceans using nadir-view OCO-2 measurements and subject it to several idealised tests. This study goes beyond (Richardson et al., 2017) by (i) considering information content aspects to select groups of channels rather than combined super-channels, (ii) accounting for local meteorological conditions and (iii) adding cloud pressure thickness to the retrieval state vector.

OCO-2 has 1,016 A-band channels of which 853 function across all soundings and here we select channels that contain the most information about the retrieved state properties, which speeds both the radiative transfer simulation and the optimal estimation calculations. The particular set of channels depends on the exact cloud case and on the across-track position of the measurement because the instrument line shapes (ILS) vary across the swath. Furthermore, neighbouring ILS overlap so it is more computationally efficient to select neighbouring pixels since the radiative transfer will already have been calculated for many of the relevant frequencies. We refer to the selection of neighbouring channels as a "micro-window" approach and use the OCO-2 Level 2 Full Physics Radiative Transfer Model (L2FP RTM, (Boesch et al., 2015)) with a set of representative atmosphere and liquid cloud states to select the optimal micro window based on information content and posterior error criteria.

The paper is organised as follows: Sect. 2 describes the OCO-2 satellite measurements, radiative transfer model and general information content approach. Sect. 3 details the methodology specific to this paper, including the sample atmospheres, perturbations for determining covariance matrix components, the sequential channel selection procedure and information content and retrieval analysis. Sect. 4 reports the results of each of these cases, Sect. 5 discusses the results and describes how they will be applied in the real OCO-2 cloud retrieval, and Sect. 6 concludes.

2 The OCO-2 satellite and its instruments

The OCO-2 satellite orbits in a Sun-synchronous orbit as part of the A-train constellation (L'Ecuyer and Jiang, 2010). It follows a 16-day repeat cycle at the Equator with a crossing time near 13:30 in the ascending node and follows the CloudSat and CALIPSO reference ground track. OCO-2 has three viewing modes: a target mode for in-flight validation plus glint and nadir modes for operational measurements. Currently the satellite alternates nadir and glint orbits with some ocean orbits dedicated entirely to glint mode. Here we use nadir soundings to allow future cross-comparisons with the nadir-view instruments on CloudSat and CALIPSO. Several nadir orbits pass over marine stratocumulus regions where these measurements offer unique value in terms of determining cloud geometric thickness, for clouds that are thick enough to attenuate and multiply scatter the CALIPSO lidar (Vaughan et al., 2009), and low enough that CloudSat suffers significantly from surface clutter (Huang et al., 2012) as well as being limited in terms of vertical resolution by the radar bin size which is downsampled to 240 m (Stephens et al., 2008). Currently, the main OCO-2 products are for column atmospheric CO2 abundance (XCO2 (Crisp, 2008; Crisp et al., 2016; Eldering et al., 2016; Osterman et al., 2016)) and solar-induced fluorescence (SIF, (Frankenberg et al., 2014)) which only use clear-sky soundings. This work therefore generates value from largely unused soundings.

OCO-2 functions in a pushbroom fashion with the footprint size depending on the viewing mode, but typically being 1.2—2.3 km. There are 8 across-track soundings, and each set of these is referred to as a frame in OCO-2 nomenclature. Within each sounding, measurements of reflected sunlight are taken in the oxygen A-band, weak-CO_2 and strong-CO_2 bands. The CO_2 bands are not considered in this analysis but do contain information about cloud phase and droplet or particle size, and this information is used when this retrieval is applied in our observation-based study to identify likely liquid cloud cases.

The OCO-2 A-band instrument is a bore-sighted, imaging, grating spectrometer that measures 1,016 channels spanning the wavelengths 759.2—771.8 nm. It is a flight spare from the original OCO mission and a number of pixels have failed. 853 of the 1,016 channels are available across all soundings and over 94 % of the damaged pixels occur in the A-band continuum where there is redundancy, meaning little loss of information (Richardson et al., 2017).

This redundancy extends to the remaining undamaged pixels, meaning that fewer channels may be used to reduce the computational burden of a retrieval. The minimum number of channels required is equal to the number of elements in the retrieval state vector, provided that the channel responses to changes in the state vector properties contain orthogonal components. Therefore, for our desired retrievals of optical depth, physical thickness and cloud-top pressure, a single cloud retrieval requires at least 3 channels. The purpose of this study is to determine how many channels are required to cover a range of realistic cloud cases and to identify those channels.

A quirk of the OCO-2 instrument complicates this determination. The wavelength of channels varies slightly between across-track soundings, which means that the sampled oxygen absorption coefficient also varies. For this reason we separately analyse each of the 8 frame sounding positions.

2.1 OCO-2 radiative transfer calculations

We use the OCO-2 Level 2 Full Physics Radiative Transfer Model (L2RTM) that was developed for the OCO-2 XCO2 retrieval. Associated wrapper code handles inputs such as interpolated ECMWF meteorological fields and accounts for the OCO-2 satellite orbit, viewing geometry and instrumental response. The radiative transfer is based on the VLIDORT radiative transfer model with a correction for the first two orders of scattering (Natraj and Spurr, 2007; Spurr, 2006; Spurr et al., 2001) that fundamentally follows the eigenvector approach to solving the radiative transfer equation (Flatau and Stephens, 1988). This model accounts for Earth's curvature for calculating atmospheric path length of the incident and reflected solar beam, but is otherwise horizontally homogeneous. More details are provided in (Spurr, 2006) and (O'Dell, 2010).

Although the L2RTM was designed for clear-sky XCO2 retrievals, it has been validated in cloudy atmospheres by comparing OCO-2 observations with L2RTM output assuming collocated MODIS and CALIPSO cloud properties (Richardson et al., 2017). For homogeneous single-layer liquid clouds over ocean, the root mean square error (RMSE) in continuum channels was ±18 %, an overestimate of the model-only error as this includes 3d cloud effects, collocation error, parallax effects and uncertainty in the MODIS and CALIPSO retrievals.

Clouds are implemented as follows: the atmosphere is defined on 20 levels, of which one is defined as the cloud centre, one as the cloud top and one as the cloud bottom. The cloud top is placed at the cloud-top pressure and the other cloud levels are

Atmos. Meas. Tech. Discuss., https://doi.org/10.5194/amt-2017-314
Manuscript under review for journal Atmos. Meas. Tech.
Discussion started: 4 October 2017

Atmospheric Measurement Techniques Discussions

equidistantly spaced to cover the cloud-pressure thickness. An extinction coefficient is assigned to the centre level to result in the desired optical depth. Above the cloud the pressure levels are linearly interpolated from the cloud top to 1 Pa. Below the cloud they are linearly interpolated from the cloud bottom to the surface pressure. The level selected for the cloud centre is that whose pressure is closest to the cloud centre when linearly interpolated across the 20 levels from the surface pressure to 1 Pa. The L2RTM assigns extinction coefficients to layers by interpolating between levels, so a vertically homogeneous cloud layer is assumed.

2.2 Optimal estimation and information content

We follow the principles of optimal estimation from (Rodgers, 2000), where a Bayesian retrieval combines an observation vector $\mathbf{y}$ with a prior state vector $\mathbf{x}_a$ and obtains a posterior state $\hat{\mathbf{x}}$. This assumes that the observation can be related to the state by a linear forward model with some error $\boldsymbol{\epsilon}$:

$$\mathbf{y} = \mathbf{K}\mathbf{x} + \boldsymbol{\epsilon} \quad (1)$$

Where we refer to $\mathbf{K}$ as the Jacobian matrix as its elements are $K_{i,j} = \partial y_i / \partial x_j$. Assuming Gaussian distributions associated with $\mathbf{x}_a$ and $\mathbf{y}$, (Rodgers, 2000) shows that the best estimate of the posterior state is:

$$\hat{\mathbf{x}} = \mathbf{x_a} + \mathbf{S_a}\mathbf{K}^T(\mathbf{K}\mathbf{S_a}\mathbf{K}^T + \mathbf{S}_\epsilon)^{-1}(\mathbf{y} - \mathbf{K}\mathbf{x_a}) \quad (2)$$

And its covariance matrix is:

$$\hat{\mathbf{S}} = \left(\mathbf{K}^T\mathbf{S}_\epsilon^{-1}\mathbf{K} + \mathbf{S}_a^{-1}\right)^{-1} \quad (3)$$

Here $\mathbf{S}_a$ is the prior covariance and $\mathbf{S}_\epsilon$ the observation covariance. From Eq. (2) the posterior state is the prior plus an iteration that is based on the observed and expected $\mathbf{y}$ with appropriate weighting for uncertainties. Eq. (3) shows that the reduction in posterior uncertainty depends on the size of the Jacobian weighted by the observation uncertainty. Potential nonlinearity in $\mathbf{y}(\mathbf{x})$ is addressed by iteration, with the linear expansion being determined about each iteration step.

In our OCO-2 cloud retrieval the state vector contains optical depth, cloud pressure thickness and cloud-top pressure while the observation state vector is any subset of the 853 valid OCO-2 A-band channels Using fewer channels reduces the computational burden, both in terms of the radiative transfer and for iterating the retrieval which would otherwise involve repeated inversion of 853×853 matrices.

It is common practice to select channels based on information content and/or degrees of freedom for signal (Chang et al., 2017; Mahfouf et al., 2015; Martinet et al., 2014; Rabier et al., 2002). The information content is based on the concept of Shannon entropy and is related to the volume of state space occupied by the probability distribution that represents our knowledge:

$$\boldsymbol{S}(\boldsymbol{P}) = -\sum_i \boldsymbol{P}(\boldsymbol{x_i}) \log_2 \boldsymbol{P}(\boldsymbol{x_i}) \quad (4)$$

It is expressed in bits, which represents the number of binary digits required to represent the possible outcomes. A retrieval decreases the probability distribution volume, and this change in associated Shannon entropy is the information content of the measurements:

Atmos. Meas. Tech. Discuss., https://doi.org/10.5194/amt-2017-314
Manuscript under review for journal Atmos. Meas. Tech.
Discussion started: 4 October 2017

$$\boldsymbol{H = S(P_0) - S(P_1)} \quad (5)$$

For multivariate Gaussian descriptions of the probability distributions, (Rodgers, 2000) shows that the information content of measurements is:

$$\boldsymbol{IC = \frac{1}{2}\ln|S_a| - \frac{1}{2}\ln|\hat{S}| = \frac{1}{2}\ln|S_a\hat{S}^{-1}|} \quad (6)$$

In our analysis we calculate information content and posterior errors for continuous micro-windows of varying size and these calculations require $\mathbf{S}_\epsilon$ and $\mathbf{S}_a$. We assume prior covariances based partially on the MODIS and CALIPSO cross-validation from (Richardson et al., 2017), and calculate the observation covariance by perturbing atmospheric profiles. The calculation of the covariances is described in Sect. 3.1 and the channel selection approach in Sect. 3.2.

While theoretically 3 channels is sufficient to retrieve 3 state vector elements, it is not clear that the same 3 channels will apply in all cases. For example, while changes in cloud-top pressure of higher clouds may lead to strong responses in channels near line cores, light in these channels may be mostly absorbed by the time it reaches lower clouds, so less-strongly absorbing channels will be preferred for lower clouds. Changes in absorption due to temperature or water vapour may also affect the relative response of radiances to cloud properties. For this purpose, we consider a variety of atmospheric and cloud properties. Necessary observation covariances are derived by perturbing atmospheric profiles and the information content and posterior covariance are used to select an optimal micro-window. Finally a retrieval is developed and tested on cloudy atmospheres where the "truth" is assigned and pseudo-observations and prior values are provided by sampling from the previously defined covariance matrices.

3 Methodology and example atmosphere and cloud states

For ease of presentation we restrict our analysis to three representative atmospheric states, three cloud heights (680 hPa, 750 hPa and 850 hPa) and three cloud optical depths (5, 10 and 25). Together, this results in 27 combination cases. Effective droplet radius is assumed to be 12 μm, and cloud-pressure thickness is determined from the cloud geometric thickness from the stratiform cloud model (Borg and Bennartz, 2007):

$$\boldsymbol{H = \sqrt{\frac{2LWP}{C_w}}} \quad (7)$$

Where C_w is the moist adiabatic condensate coefficient and for marine stratocumulus we use 1.9×10^{-3} g m^{-4} (range given as 1—2.5×10^{-3} g m^{-4} from (Brenguier, 1991) and LWP is the liquid water path which is related to optical depth τ and effective droplet radius r_{eff}:

$$\boldsymbol{LWP = \frac{\tau r_{eff} 10\rho}{9Q_{ext}}} \quad (8)$$

Atmos. Meas. Tech. Discuss., https://doi.org/10.5194/amt-2017-314
Manuscript under review for journal Atmos. Meas. Tech.
Discussion started: 4 October 2017

Atmospheric Measurement Techniques Discussions

Where ρ_w is the density of water and Q_{ext} the area-weighted mean scattering efficiency (Szczodrak et al., 2001), which we take to be 2. A pressure scale height of 8 km is assumed to convert the resultant cloud geometric thickness to pressure thickness. Note that this result comes from an adiabatic cloud model in which the LWP increases linearly with height, and differs by a factor of 5/6 from the classic result derived for a homogeneous cloud profile (Stephens, 1978). Neither assumption is perfectly representative of reality, but the adiabatic profile is expected to be more realistic so is used here.

For the representative atmospheric states, we select all soundings that are identified as single-layer liquid clouds by both MODIS and CALIPSO during November 2015 and bin them according to absolute latitude, in the ranges 0—20°, 20—50° and 50—90°. Then the OCO-2 ECMWF-AUX meteorological profiles assigned to each of these soundings are taken and within each bin all of the profiles are averaged level-by-level. This includes all meteorological inputs used by the L2RTM, such as pressure, temperature, humidity and wind speed.

3.1 Calculation of observation covariances

For simplicity we assume that the components of $\mathbf{S}_\epsilon$ are independent and consider error contributions from instrumental uncertainty $\mathbf{S}_I$, and that introduced by uncertainty in the temperature profile $\mathbf{S}_T$, humidity profile $\mathbf{S}_q$ and effective droplet radius $\boldsymbol{S}_{reff}$ such that:

$$\mathbf{S}_\epsilon = \mathbf{S}_I + \mathbf{S}_T + \mathbf{S}_q + \mathbf{S}_{reff} \quad (9)$$

In reality, the temperature and humidity uncertainties are likely to be correlated, but this simplifies the calculation and allows unique attribution of covariance sources. The matrix $\mathbf{S}_I$ is a diagonal matrix so averaging over more channels reduces the total posterior uncertainty even if the Jacobians are not independent. Its elements are equal to the square of the instrumental uncertainty, which depends on the radiance.

For $\mathbf{S}_T$ and $\mathbf{S}_q$ we follow the approach of (Chang et al., 2017) and perturb the tropical, mid-latitude and high-latitude atmospheric profiles 2,000 times for temperature or humidity separately. Uncertainties are based on the 1 km resolution AIRS validation results (Divakarla et al., 2006) and are ±1.5 K in temperature and for specific humidity, scale linearly from ±20 % at the surface to ±50 % at 250 hPa. At higher altitudes, ±50 % is used at all levels. For each perturbed temperature simulation, the entire temperature profile is uniformly perturbed by a single value sampled from a zero-mean Gaussian with standard deviation ±1.5 K. For specific humidity, we sample from a zero-mean Gaussian with unit standard deviation and multiply that value by the percentage scaling profile described above. The calculation was also performed with 2,000 perturbations to r_{eff} assuming a lognormal distribution with a mean of 12.6 μm and 5—95 % range of 7.5—19.4 μm.

For each set of perturbations, we simulated the A-band spectra for cloud optical depths of 5, 10 and 25 and solar zenith angles of approximately 30°, 45° and 60° with a cloud-top pressure of 850 hPa. The output was sampled with each of the 8 different instrument line shapes associated with the 8 different OCO-2 across-track sounding positions.

For each set of 2,000 perturbed outputs, we estimated the covariance matrix elements, $S_{i,j}$, where i, j refer to channel indices, as:

Atmos. Meas. Tech. Discuss., https://doi.org/10.5194/amt-2017-314
Manuscript under review for journal Atmos. Meas. Tech.
Discussion started: 4 October 2017

Atmospheric Measurement Techniques Discussions

$$\boldsymbol{S_{i,j}} = \sum_{\boldsymbol{k}}(\boldsymbol{I_{i,k}} - < \boldsymbol{I_i} >)(\boldsymbol{I_{j,k}} - < \boldsymbol{I_j} >)/\boldsymbol{N} \quad (10)$$

Where the sum is over the N=2,000 spectra of radiance I, which are individually referred to using the index k. In this case $< I_i >$ and $< I_j >$ are the sample mean radiances in the relevant pixels i and j.

3.2 Channel selection

Eq. (3) and Eq. (6) state that we can determine the information content and posterior error covariance from the prior covariance, observation covariance and Jacobians. Our aim is to select the optimal micro-window of consecutive OCO-2 pixels to provide a retrieval that efficiently reduces the posterior state error.

We use the L2FP radiative transfer model to simulate OCO-2 spectra for marine liquid clouds of τ in [5, 10, 25] and $\underline{P_{top}}$ in [680, 750, 850] hPa, for each of the 3 meteorological cases in Sect. 3.1 and for each of the eight across-track sounding positions. In each case, the solar zenith angle is 45° and the Jacobians for τ, P_{top} and ΔP are determined by finite differencing. The relevant observation covariance is that determined for the same sounding position, region and optical depth in Sect. 2.2 at SZA = 45°. Prior covariance is assumed to be diagonal, equivalent to τ error of ±1.5, P_{top} of ±60 hPa and ΔP of ±7.5 hPa. Our τ prior error comes from applying the ±15 % error in simulated radiance for homogeneous clouds when provided with MODIS optical depth found in (Richardson et al., 2017). Our P_{top} uncertainty is approximately equal to that determined in the same study when comparing prior OCO-2 P_{top} with CALIPSO. The ΔP uncertainty is similar to the ±20 % error associated with Eq. (7) for clouds of cloud fraction > 0.8 reported in (Bennartz, 2007).

We consider the information content IC, and the 3 diagonal elements of the posterior covariance matrix $\mathbf{S}_x$. The information content accounts for non-diagonal terms in the posterior covariance, allowing an objective best selection, while the diagonal elements allow more intuitive interpretation of the magnitude of the posterior uncertainty. We refer to these using the symbol σ with a relevant subscript, such that $\sigma_\tau^2 = S_{\tau,\tau}$ where $S_{\tau,\tau}$ is the element of the covariance matrix corresponding to the $\tau - \tau$ covariance. Note that we present the square-root of this value, i.e. σ.

This approach represents a sample of 27 unique cloud-meteorology cases across the 8 different sets of OCO-2 instrument line shapes, resulting in 216 total cases. When selecting the optimal micro-window for retrievals, it is necessary to select not just its location, but also its size (i.e. number of neighbouring pixels within the micro-window).

To make this problem tractable, we select micro-windows of the following size: 5, 10, 25, 50, 75, 100, 150, 200, 500. For each of these possible sizes we calculate IC and the diagonal posterior error terms for every overlapping micro-window of that size. For example, the 853 individual OCO-2 pixels allow 849 overlapping 5-pixel micro-windows, for which we determine the information content values for each of the 216 cases.

For each size of micro-window we choose the one with the highest mean information content across the 216 cases. This may result in a different location for each size of micro-window, and we select the optimal micro-window size as that with >80 % of the 500-channel IC, optical depth posterior $\sigma_{\tau,\tau}$ better than ±0.05 and a posterior of better than ±1 hPa in the pressure terms $\sigma_{P_{top},P_{top}}$ and $\sigma_{\Delta P,\Delta P}$ for all 216 cases.

Atmos. Meas. Tech. Discuss., https://doi.org/10.5194/amt-2017-314
Manuscript under review for journal Atmos. Meas. Tech.
Discussion started: 4 October 2017

Atmospheric Measurement Techniques Discussions

3.3 Theoretical retrieval test case

We perform synthetic retrievals with known true cloud cases in mid-latitude meteorology and a 45° solar zenith angle. For each cloud case we perform 50 retrievals using a 12 micron droplet size and the prior cloud state is sampled from Gaussian distributions with σ_τ of ±30 %, $\sigma_{P_{top}}$ of ±60 hPa. Cloud pressure thickness is calculated from Eq. (7) with LWP from Eq. (8), and in the optimal estimation a prior $\sigma_{\Delta P}$ of ±25 % is assumed. The atmospheric humidity and temperature profiles are perturbed by sampling from the same distributions used to derive the covariance matrices in Sect. 3.2 and the observed spectrum in each case is generated by taking the simulated spectrum from the "truth" case and perturbing it by sampling from the relevant covariance matrix that has been scaled for the cloud properties according to Sect. 3.2.

Forty true cloud cases are used with five of each case where optical depth ranges from 5 to 40 in increments of 5 and cloud-top pressure is randomly selected to be between 680—900 hPa and rounded to the nearest 10 hPa. The retrieval attempts assume r_{eff} = 12 μm but the true r_{eff} is allowed to vary and is randomly sampled from a literature summary of marine stratocumulus results, scaled to ensure a mean value of 12 μm (Miles et al., 2000).

For each of the 50 perturbed prior states and observation spectra, we perform a standard 10-iteration optimal estimation retrieval (Rodgers, 2000) using the Gauss-Newton solution to optimise each step. These retrievals are done using the micro-window selected following Sect. 3.3. The sample means and standard deviations are then compared with the known true state and indicate the theoretical performance of the micro-window retrieval.

4 Results

Results are presented here for the first sounding position, which is left-most when facing northwards along track during the ascending node. Our conclusions are not affected by changing the sounding position. For illustration, we select the case of SZA = 45°, τ = 10 and P_{top} = 850 hPa then present the square root of the diagonal components of covariance matrices for temperature, humidity and effective radius in Figure 1. This shows both the absolute and fractional uncertainty in the radiance due to each factor. Droplet size dominates, consistently contributing near 3 % of the radiance, although the temperature uncertainty contributes up to 1.5 % in the darker absorption channels.

Figure 2 shows the full covariance matrices for each component using the mid-latitude meteorology and the same cloud and SZA as Figure 1. The strongest and most consistent positive cross-correlations occur for the effective droplet size.

While the overall patterns are similar for different cloud optical depths, solar zenith angles or regional meteorology, the absolute values of the covariance matrices change. A retrieval requires an estimate of the error covariance that is relevant for the given measurement but these matrices are computationally intensive to prepare, and storing and accessing a large number of them would make the retrieval less efficient. We will therefore use a single set of retrieval matrices, one for each across-track sounding position, and then scale the matrix to account for changes in solar zenith angle, meteorology and optical depth.

Atmos. Meas. Tech. Discuss., https://doi.org/10.5194/amt-2017-314
Manuscript under review for journal Atmos. Meas. Tech.
Discussion started: 4 October 2017

Atmospheric Measurement Techniques Discussions

Figure 3 shows the relationship between the observation covariance matrix ecluding the instrumental term $\mathbf{S}_I$ for τ = 10, SZA = 30° and τ = 25, SZA = 60° with mid-latitude meteorology. Only the upper-diagonal elements of each matrix have been plotted to avoid duplication and values are scaled by μ^{-2}, where $\mu = \cos\theta_{SZA}$. There is a linear relationship between the two matrices meaning that one may be reconstructed from the other. The results are similar for tropical and high-latitude cases, and for all soundings.

4.2 Micro-window selection

Figure 4 shows information content spectra using micro-windows consisting of 5, 75 or 200 OCO-2 pixels. Also shown are the posterior errors in cloud properties taken from the square roots of the diagonal components of $\mathbf{S}_x$.

In this cloud case (mid latitude, τ = 10, P_{top} = 850 hPa), the greatest information content comes from selecting channels near absorption features and avoiding the far wings of the A-band where only optical depth is reliably retrieved, as these channels have little O_2 absorption and so are uninformative about photon path length. Otherwise, the 5-pixel micro-window is most sensitive to its placement within the spectrum: information content varies from 4.4—9.4 bits depending on the micro-window's location.

Micro-windows that contain fewer pixels are more sensitive to changes in the instrument line shapes and cloud conditions. For example, for the 5-pixel micro-window in Figure 4, the best-performing channel has an information content of 9.4 bits. However, for a different cloudy case: τ = 25, P_{top} = 680 hPa, and for sounding position 8 instead of 1, the information content is reduced to 6.0 bits. This is a substantial loss relative to the best possible micro-window for that cloud case, which has 8.4 bits of information.

To assess the relative trade-offs between increased speed and decreased performance we take the micro-window with the highest mean information content2. We then plot the central value and full range of the 216 values for each selected micro-window size in Figure 5, along with our chosen thresholds as dashed lines in each panel. The 75 pixel micro-window containing the OCO-2 pixels 353—426 (indices counting from 1 for the full 1,016 OCO-2 L1bSc pixels) satisfies our criteria and reduces the full wavelength range from 759.2—771.8 nm to 763.5—764.6 nm.

4.3 Theoretical retrieval case

Example synthetic retrieval iterations using the 75-channel micro-window are shown in Figure 6 for $\tau = 10$ and $\tau = 25$ cases, and convergence typically occurs within few iterations. Lines are coloured according to their χ^2 values and it is clear that this is larger for cases where the result settles away from the true state. The posterior sample standard deviations are presented in Table 1 for the full samples and for cases where we filter the results by excluding the 10 % of cases with the highest χ^2 in each case. The greatest effect of filtering by χ^2 is to reduce the uncertainty in the cloud-top pressure and cloud pressure thickness from 12.9 hPa to 2.9 hPa and 2.5 hPa respectively. The mean standard deviation in the τ retrieval is ±0.75 across all cases, but this is inflated by a large value in the τ = 35 cases.

Atmos. Meas. Tech. Discuss., https://doi.org/10.5194/amt-2017-314
Manuscript under review for journal Atmos. Meas. Tech.
Discussion started: 4 October 2017

5 Discussion

OCO-2 O_2 A-band spectra are rich in information about cloud properties. Continuum pixels with little absorption respond strongly to cloud optical depth, while the radiance in absorption bands is dominated by photon path length, which increases with cloud-top pressure or cloud pressure thickness. The response to cloud properties depends largely on the oxygen absorption coefficient in the given channel (Fischer and Grassl, 1991b; Koelemeijer et al., 2001; Stephens and Heidinger, 2000), and with many pixels having similar oxygen absorption coefficients, there is much redundant cloud information in OCO-2 spectra.

We ultimately selected 75 neighbouring channels as containing the majority of the cloud information. Observation covariance matrices were developed based on uncertainty related to the atmospheric temperature and humidity profiles, in cloud droplet effective radius and instrumental uncertainty. These covariances depend on the meteorological profile, solar zenith angle and cloud properties, and that as instrument line shapes vary across the OCO-2 swath, a separate covariance matrix is required for each of the eight across-track OCO-2 footprints. Fortunately, when cloud or meteorological properties change, the covariance matrix elements tend to be approximately linearly related, allowing an arbitrary covariance matrix to be reconstructed from the covariance matrix for a known case. There is greater spread in the reconstructed humidity component but this contributes a small fraction of the total covariance, which is dominated by uncertainty in the droplet radius, whose component is well reconstructed.

Using 75 channels substantially reduces the retrieval processing time relative to the 853 available channels, and its usefulness was demonstrated in a set of 8 synthetic test cases where a known cloud case was retrieved. In our perturbed tests the retrieval typically converged within 2 iterations, although a few cases converged on a local optimum instead of approaching the truth. Fortunately, these cases can generally be identified from the associated χ^2, indicating that when this approach is applied to real OCO-2 data, it may be possible to flag cases where there is less confidence in the retrieval.

Our idealised posterior errors of ±0.75 in optical depth and better than ±3 hPa in cloud-top pressure and cloud pressure thickness are based on assuming that convergence can be identified from the χ^2 values, and that the cloud is single-layered and horizontally homogeneous within the OCO-2 field of view of approximately 1.4×2.2 km. This is a reasonable approximation in marine stratocumulus decks, where the typical length scale of variability in Liquid Water Path can be 10—30 km (Wood and Hartmann, 2006), but will be violated in many low level cloud cases such as at the edges of the stratocumulus-trade cumulus transition. In addition, multi-layered clouds are ubiquitous (Li et al., 2015), although for overlying cirrus it may be possible to identify and flag many of these cases based on the inferred distribution of photon path lengths from A-band measurements (Min et al., 2004).

It was also assumed that the clouds will be reliably identified as liquid, and that a constant effective droplet size may be assumed. Droplet size variance has been included in terms of the observation covariance, but this limits our retrieved posterior covariance. The OCO-2 instrument also carries weak- and strong-CO2 band spectrometers, and with ice absorbing more strongly than water in the near infrared we will be able to use well-known retrieval principles to obtain cloud phase (Nakajima and King, 1990).

Our assumptions mean that the true error of an OCO-2 based cloud retrieval will be larger than that reported here, but our results suggest that the use of a 75-channel micro-window is justified as the basis of an OCO-2 cloud retrieval for marine liquid cloud properties.

6 Conclusions

The OCO-2 satellite carries an O_2 A-band spectroradiometer with high spectral sampling in terms of oxygen absorption coefficient. Our analysis supports that this spectral sampling is sufficient to, in principle, allow determination of the optical depth, cloud-top pressure and geometric pressure thickness of clouds. It has been demonstrated that observed OCO-2 spectra respond largely as expected to changes in cloud optical depth and cloud-top pressure (Richardson et al., 2017), but that study did not use modern Bayesian techniques. Such techniques account for relevant conditions such as line broadening due to local meteorology and they also account for prior information and cross-correlation between the responses of individual channels.

Here we report that the OCO-2 A-band spectra contain much redundant information as a number of channels experience similar oxygen absorption. After accounting for observational errors associated with uncertainty introduced by meteorology, cloud droplet size and instrumental error, it was found that with a micro-window of 75 continuous channels, most of the information from the full 853-channel spectrum is retained. In a perfectly linear theoretical case, posterior error in cloud-top pressure and cloud pressure thickness were reduced below ±1 hPa and optical depth below ±0.05.

Using perturbed synthetic tests, the majority of cases approached the known truth and the full sample posterior errors averaged ±0.75 in optical depth, ±12.9 hPa in P_{top} and cloud pressure thickness. Cases that converged to a state away from the truth could generally be identified by their large χ^2 values, and removing the 10 % of worst cases reduced the posterior sample standard deviation in P_{top} and ΔP_c was reduced to ±2.9 and ±2.5 hPa.

These results apply in an ideal theoretical case of a uniform single layer liquid droplet cloud, and retrieval errors will be larger in reality where these assumptions do not apply. However, violations of these assumptions such as real-world cloud heterogeneity, will likely have a similar effect on both the full spectrum and on our selected 75-channel micro-window. We therefore propose that these assumptions do not affect our primary conclusion regarding the relative performance of our optimised retrieval versus a more intensive, full spectrum retrieval.

Acknowledgments This research described in this paper was performed at the Jet Propulsion Laboratory, California Institute of Technology sponsored by NASA. MR has been funded by the OCO-2 and CloudSat projects. MR would like to thank James McDuffie and Jussi Leinonen for providing radiative transfer and optimal estimation code assistance, plus Matt Lebsock, Annmarie Eldering, Mike Gunson, Chris O'Dell, Tommy Taylor, Heather Cronk and Aronne Merrelli for helpful technical discussions. The OCO-2 science data are available online from the NASA Goddard GES DISC at https://disc.gsfc.nasa.gov/datacollection/OCO2_L1B_Science_7.html.

References

Baum, B. A., Menzel, W. P., Frey, R. A., Tobin, D. C., Holz, R. E., Ackerman, S. A., Heidinger, A. K. and Yang, P.: MODIS Cloud-Top Property Refinements for Collection 6, J. Appl. Meteorol. Climatol., 51(6), 1145–1163, doi:10.1175/JAMC-D-11-0203.1, 2012.

Bennartz, R.: Global assessment of marine boundary layer cloud droplet number concentration from satellite, J. Geophys. Res., 112(D2), D02201, doi:10.1029/2006JD007547, 2007.

Boesch, H., Brown, L., Castano, R., Christi, M., Connor, B., Crisp, D., Eldering, A., Fisher, B., Frankenberg, C., Gunson, M., Granat, R., McDuffie, J., Miller, C., Natraj, V., O'Brien, D., O'Dell, C., Osterman, G., Oyafuso, F., Payne, V., Polonsky, I., Smyth, M., Spurr, R., Thompson, D. and Toon, G.: Orbiting Carbon Observatory (OCO)-2 Level 2 Full Physics Algorithm Theoretical Basis Document, Pasadena, CA. [online] Available from: https://disc.gsfc.nasa.gov/OCO-2/documentation/oco-2-v6/OCO2_L2_ATBD.V6.pdf, 2015.

Borg, L. A. and Bennartz, R.: Vertical structure of stratiform marine boundary layer clouds and its impact on cloud albedo, Geophys. Res. Lett., 34(5), doi:10.1029/2006GL028713, 2007.

Brenguier, J.: Parameterization of the Condensation Process: A Theoretical Approach, J. Atmos. Sci., 48(2), 264–282, doi:10.1175/1520-0469(1991)048<0264:POTCPA>2.0.CO;2, 1991.

Chang, K.-W., L'Ecuyer, T. S., Kahn, B. H. and Natraj, V.: Information content of visible and midinfrared radiances for retrieving tropical ice cloud properties, J. Geophys. Res. Atmos., 122(9), 4944–4966, doi:10.1002/2016JD026357, 2017.

Crisp, D.: NASA Orbiting Carbon Observatory: measuring the column averaged carbon dioxide mole fraction from space, J. Appl. Remote Sens., 2(1), 23508, doi:10.1117/1.2898457, 2008.

Crisp, D., Pollock, H. R., Rosenberg, R., Chapsky, L., Lee, R. A. M., Oyafuso, F. A., Frankenberg, C., O'Dell, C. W., Bruegge, C. J., Doran, G. B., Eldering, A., Fisher, B. M., Fu, D., Gunson, M. R., Mandrake, L., Osterman, G. B., Schwandner, F. M., Sun, K., Taylor, T. E., Wennberg, P. O. and Wunch, D.: The On-Orbit Performance of the Orbiting Carbon Observatory-2 (OCO-2) Instrument and its Radiometrically Calibrated Products, Atmos. Meas. Tech. Discuss., 1–45, doi:10.5194/amt-2016-281, 2016.

Divakarla, M. G., Barnet, C. D., Goldberg, M. D., McMillin, L. M., Maddy, E., Wolf, W., Zhou, L. and Liu, X.: Validation of Atmospheric Infrared Sounder temperature and water vapor retrievals with matched radiosonde measurements and forecasts, J. Geophys. Res., 111(D9), D09S15, doi:10.1029/2005JD006116, 2006.

Eldering, A., O'Dell, C. W., Wennberg, P. O., Crisp, D., Gunson, M. R., Viatte, C., Avis, C., Braverman, A., Castano, R., Chang, A., Chapsky, L., Cheng, C., Connor, B., Dang, L., Doran, G., Fisher, B., Frankenberg, C., Fu, D., Granat, R., Hobbs, J., Lee, R. A. M., Mandrake, L., McDuffie, J., Miller, C. E., Myers, V., Natraj, V., O'Brien, D., Osterman, G. B., Oyafuso, F., Payne, V. H., Pollock, H. R., Polonsky, I., Roehl, C. M., Rosenberg, R., Schwandner, F., Smyth, M., Tang, V., Taylor, T. E., To, C., Wunch, D. and Yoshimizu, J.: The Orbiting Carbon Observatory-2: First 18 months of Science Data Products, Atmos. Meas. Tech.

Discuss., 1–30, doi:10.5194/amt-2016-247, 2016.

Fischer, J. and Grassl, H.: Detection of Cloud-Top Height from Backscattered Radiances within the Oxygen A Band. Part 1: Theoretical Study, J. Appl. Meteorol., 30(9), 1245–1259, doi:10.1175/1520-0450(1991)030<1245:DOCTHF>2.0.CO;2, 1991a.

Fischer, J. and Grassl, H.: Detection of Cloud-Top Height from Backscattered Radiances within the Oxygen A Band. Part 1: Theoretical Study, J. Appl. Meteorol., 30(9), 1245–1259, doi:10.1175/1520-0450(1991)030<1245:DOCTHF>2.0.CO;2, 1991b.

Flatau, P. J. and Stephens, G. L.: On the fundamental solution of the radiative transfer equation, J. Geophys. Res., 93(D9), 11037, doi:10.1029/JD093iD09p11037, 1988.

Frankenberg, C., O'Dell, C., Berry, J., Guanter, L., Joiner, J., Köhler, P., Pollock, R. and Taylor, T. E.: Prospects for chlorophyll fluorescence remote sensing from the Orbiting Carbon Observatory-2, Remote Sens. Environ., 147, 1–12, doi:10.1016/j.rse.2014.02.007, 2014.

Huang, Y., Siems, S. T., Manton, M. J., Hande, L. B. and Haynes, J. M.: The Structure of Low-Altitude Clouds over the Southern Ocean as Seen by CloudSat, J. Clim., 25(7), 2535–2546, doi:10.1175/JCLI-D-11-00131.1, 2012.

Koelemeijer, R. B. A., Stammes, P., Hovenier, J. W. and de Haan, J. F.: A fast method for retrieval of cloud parameters using oxygen A band measurements from the Global Ozone Monitoring Experiment, J. Geophys. Res. Atmos., 106(D4), 3475–3490, doi:10.1029/2000JD900657, 2001.

L'Ecuyer, T. S. and Jiang, J. H.: Touring the atmosphere aboard the A-Train, Phys. Today, 63(7), 36–41, doi:10.1063/1.3463626, 2010.

Li, J., Huang, J., Stamnes, K., Wang, T., Lv, Q. and Jin, H.: A global survey of cloud overlap based on CALIPSO and CloudSat measurements, Atmos. Chem. Phys., 15(1), 519–536, doi:10.5194/acp-15-519-2015, 2015.

Mahfouf, J.-F., Birman, C., Aires, F., Prigent, C., Orlandi, E. and Milz, M.: Information content on temperature and water vapour from a hyper-spectral microwave sensor, Q. J. R. Meteorol. Soc., 141(693), 3268–3284, doi:10.1002/qj.2608, 2015.

Martinet, P., Lavanant, L., Fourri?, N., Rabier, F. and Gambacorta, A.: Evaluation of a revised IASI channel selection for cloudy retrievals with a focus on the Mediterranean basin, Q. J. R. Meteorol. Soc., 140(682), 1563–1577, doi:10.1002/qj.2239, 2014.

Miles, N. L., Verlinde, J. and Clothiaux, E. E.: Cloud Droplet Size Distributions in Low-Level Stratiform Clouds, J. Atmos. Sci., 57(2), 295–311, doi:10.1175/1520-0469(2000)057<0295:CDSDIL>2.0.CO;2, 2000.

Min, Q.-L., Harrison, L. C., Kiedron, P., Berndt, J. and Joseph, E.: A high-resolution oxygen A-band and water vapor band spectrometer, J. Geophys. Res., 109(D2), D02202, doi:10.1029/2003JD003540, 2004.

Nakajima, T. and King, M. D.: Determination of the Optical Thickness and Effective Particle Radius of Clouds from Reflected Solar Radiation Measurements. Part I: Theory, J. Atmos. Sci., 47(15), 1878–1893, doi:10.1175/1520-0469(1990)047<1878:DOTOTA>2.0.CO;2, 1990.

Natraj, V. and Spurr, R. J. D.: A fast linearized pseudo-spherical two orders of scattering model to account for polarization in vertically inhomogeneous scattering–absorbing media, J. Quant. Spectrosc. Radiat. Transf., 107(2), 263–293,

doi:10.1016/j.jqsrt.2007.02.011, 2007.

O'Dell, C. W.: Acceleration of multiple-scattering, hyperspectral radiative transfer calculations via low-streams interpolation, J. Geophys. Res., 115(D10), D10206, doi:10.1029/2009JD012803, 2010.

Osterman, G. B., Eldering, A., Avis, C., Chafin, B., O'Dell, C. W., Frankenberg, C., Fisher, B. M., Mandrake, L., Wunch, D., Granat, R. and Crisp, D.: Orbiting Carbon Observatory-2 (OCO-2) Data Product User's Guide, Operational L1 and L2 Data Versions 7 and 7R, Pasadena, CA., 2016.

Rabier, F., Fourrié, N., Chafaï, D. and Prunet, P.: Channel selection methods for Infrared Atmospheric Sounding Interferometer radiances, Q. J. R. Meteorol. Soc., 128(581), 1011–1027, doi:10.1256/0035900021643638, 2002.

Richardson, M., McDuffie, J., Stephens, G. L., Cronk, H. Q. and Taylor, T. E.: The OCO-2 oxygen A-band response to liquid marine cloud properties from CALIPSO and MODIS, J. Geophys. Res. Atmos., doi:10.1002/2017JD026561, 2017.

Rodgers, C. D.: Inverse Methods for Atmospheric Sounding Theory and Practice, World Scientific, Singapore., 2000.

Spurr, R. J. D.: VLIDORT: A linearized pseudo-spherical vector discrete ordinate radiative transfer code for forward model and retrieval studies in multilayer multiple scattering media, J. Quant. Spectrosc. Radiat. Transf., 102(2), 316–342, doi:10.1016/j.jqsrt.2006.05.005, 2006.

Spurr, R. J. D., Kurosu, T. P. and Chance, K. V.: A linearized discrete ordinate radiative transfer model for atmospheric remote-sensing retrieval, J. Quant. Spectrosc. Radiat. Transf., 68(6), 689–735, doi:10.1016/S0022-4073(00)00055-8, 2001.

Stephens, G. and Heidinger, A.: Molecular Line Absorption in a Scattering Atmosphere. Part I: Theory, J. Atmos. Sci., 57(10), 1599–1614, doi:10.1175/1520-0469(2000)057<1599:MLAIAS>2.0.CO;2, 2000.

Stephens, G. L.: Radiation Profiles in Extended Water Clouds. II: Parameterization Schemes, J. Atmos. Sci., 35(11), 2123–2132, doi:10.1175/1520-0469(1978)035<2123:RPIEWC>2.0.CO;2, 1978.

Stephens, G. L., Vane, D. G., Tanelli, S., Im, E., Durden, S., Rokey, M., Reinke, D., Partain, P., Mace, G. G., Austin, R., L'Ecuyer, T., Haynes, J., Lebsock, M., Suzuki, K., Waliser, D., Wu, D., Kay, J., Gettelman, A., Wang, Z. and Marchand, R.: CloudSat mission: Performance and early science after the first year of operation, J. Geophys. Res., 113, D00A18, doi:10.1029/2008JD009982, 2008.

Szczodrak, M., Austin, P. H. and Krummel, P. B.: Variability of Optical Depth and Effective Radius in Marine Stratocumulus Clouds, J. Atmos. Sci., 58(19), 2912–2926, doi:10.1175/1520-0469(2001)058<2912:VOODAE>2.0.CO;2, 2001.

Taylor, T. E., O'Dell, C. W., Frankenberg, C., Partain, P. T., Cronk, H. Q., Savtchenko, A., Nelson, R. R., Rosenthal, E. J., Chang, A. Y., Fisher, B., Osterman, G. B., Pollock, R. H., Crisp, D., Eldering, A. and Gunson, M. R.: Orbiting Carbon Observatory-2 (OCO-2) cloud screening algorithms: validation against collocated MODIS and CALIOP data, Atmos. Meas. Tech., 9(3), 973–989, doi:10.5194/amt-9-973-2016, 2016.

Vaughan, M. A., Powell, K. A., Winker, D. M., Hostetler, C. A., Kuehn, R. E., Hunt, W. H., Getzewich, B. J., Young, S. A., Liu, Z. and McGill, M. J.: Fully Automated Detection of Cloud and Aerosol Layers in the CALIPSO Lidar Measurements, J. Atmos.

Ocean. Technol., 26(10), 2034–2050, doi:10.1175/2009JTECHA1228.1, 2009.

Wood, R. and Hartmann, D. L.: Spatial Variability of Liquid Water Path in Marine Low Cloud: The Importance of Mesoscale Cellular Convection, J. Clim., 19(9), 1748–1764, doi:10.1175/JCLI3702.1, 2006.

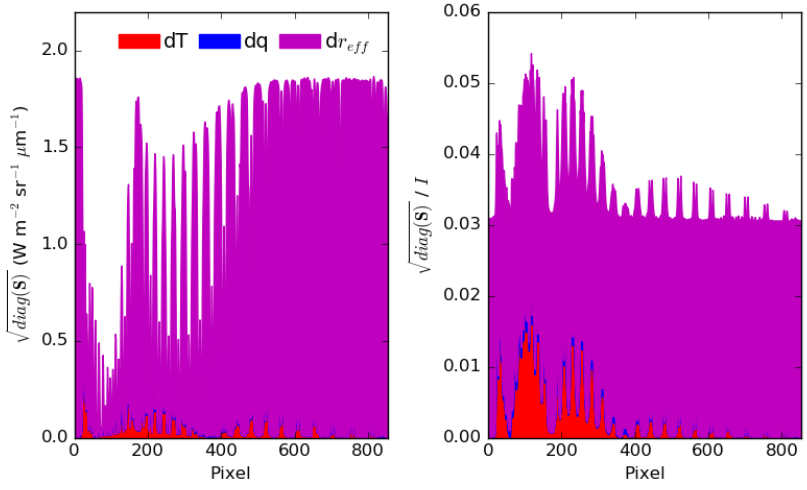

Figure 1 Square-root of diagonal components of the covariance matrix, stacked contribution from temperature (red), humidity (blue) and effective radius (magenta). Results shown for a cloud with τ = 10 and P_{top} = 850 hPa. Left shows the value in absolute radiance, and right as a fraction of the unperturbed radiance such that 0.03 represents an uncertainty of ±3 %.

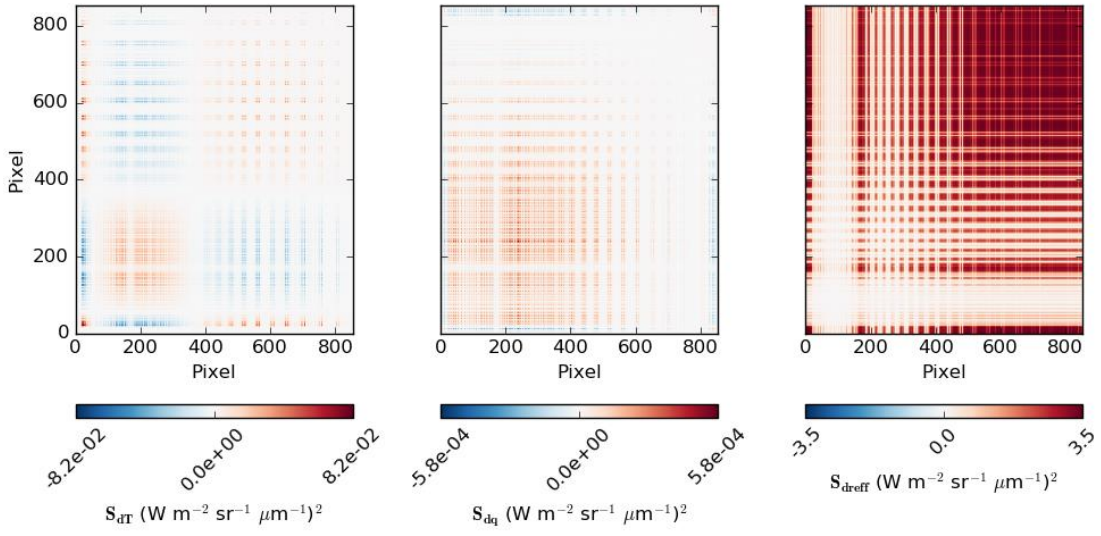

Figure 2 Example covariance matrices for each component as labelled in the colour bar: (left) temperature, (middle) humidity, (right) effective radius.

Atmos. Meas. Tech. Discuss., https://doi.org/10.5194/amt-2017-314
Manuscript under review for journal Atmos. Meas. Tech.
Discussion started: 4 October 2017

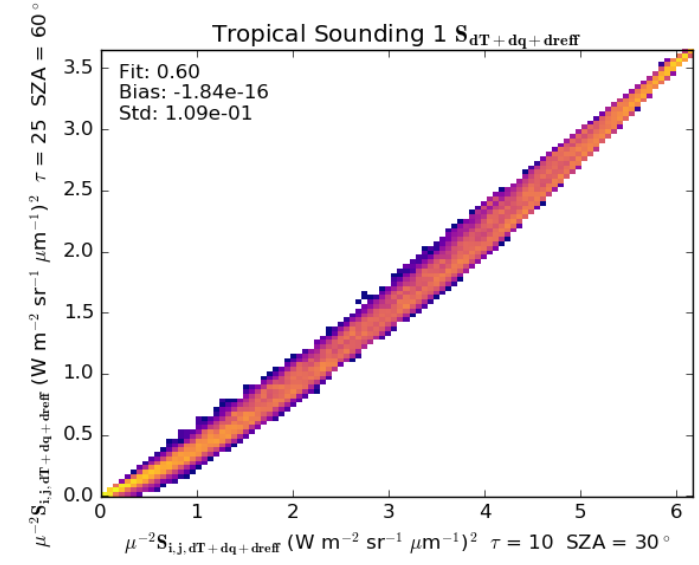

Figure 3 (top) 2d histograms of raw covariance matrix elements at 60° solar zenith angle as a function of the same values at 30° solar zenith angle for the mid-latitude meteorological state. (bottom) as top, but each value has been scaled by $\mu^{-2} = cos^{-2}(SZA)$ to account for differences in illumination geometry.

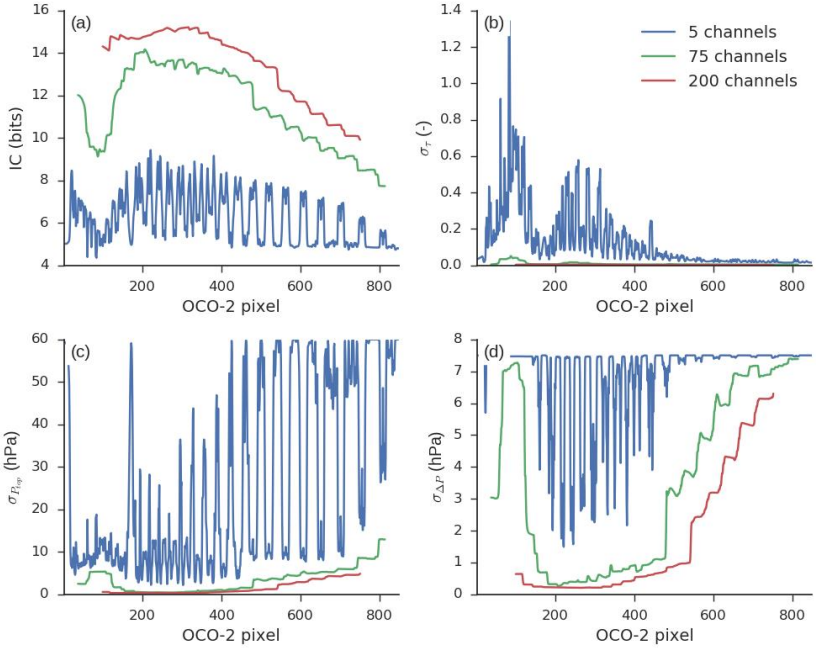

Figure 4 Results of information content analysis for a $\tau = 10$ and P_{top} = 850 hPa cloud in mean mid-latitude meteorology for OCO-2 sounding position 1. Each line represents the result using a micro-window of difference size, centred on the OCO-2 pixel given in

Atmos. Meas. Tech. Discuss., https://doi.org/10.5194/amt-2017-314
Manuscript under review for journal Atmos. Meas. Tech.
Discussion started: 4 October 2017

Atmospheric Measurement Techniques Discussions

the x-axis. Values are as follows: (a) information content in bits, (b—d) square root of diagonal elements of posterior state covariance matrix, (b) cloud optical depth, (c) cloud-top pressure and (d) cloud pressure thickness.

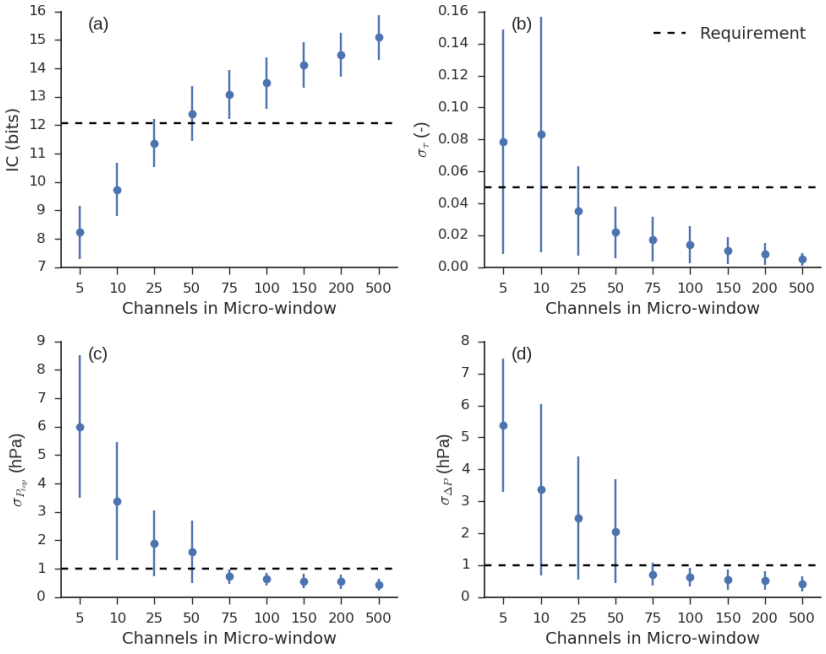

Figure 5 Range of performance for best-located micro-window of each size. The point represents the central value and the lines the full range of the 216 outputs covering each sounding position, meteorology and cloud case. Note that the x-axis is non-linear. (a) Information content in bits, (b—d) square root of diagonal covariance matrix elements: (b) cloud optical depth, (c) cloud-top pressure and (d) cloud pressure thickness. Dashed lines represent selected retrieval requirements.

Atmos. Meas. Tech. Discuss., https://doi.org/10.5194/amt-2017-314
Manuscript under review for journal Atmos. Meas. Tech.
Discussion started: 4 October 2017

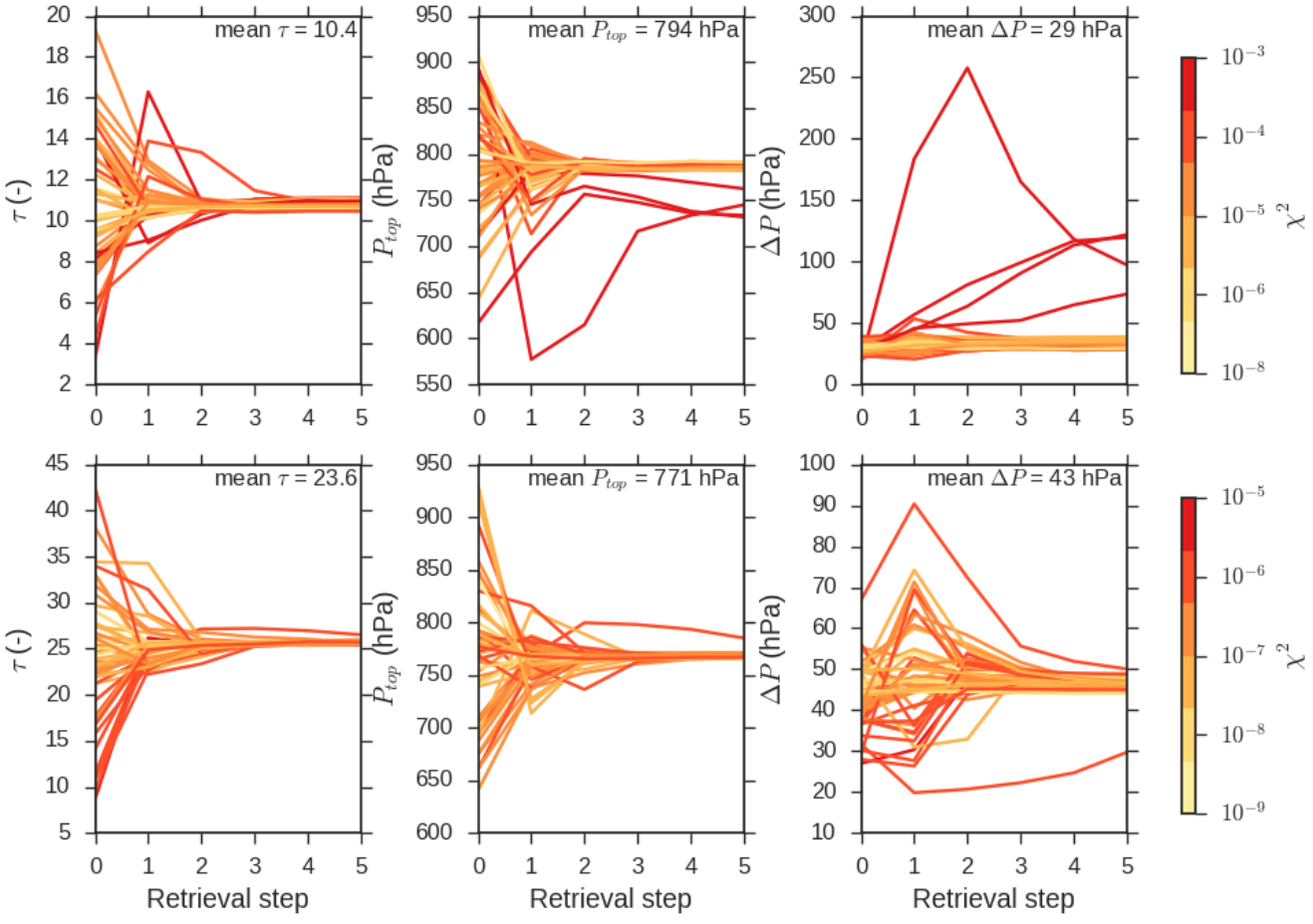

Figure 6 Example iteration in retrieved cloud properties for synthetic micro-window retrievals for test cases with cloud optical depth near 10 (top) and 25 (bottom). Each line represents the iterations through one of the 50 sample retrievals. The lines are coloured according to their χ^2 values, note the separate colour bars for the top and bottom rows with larger χ^2 for the top cases.

Atmos. Meas. Tech. Discuss., https://doi.org/10.5194/amt-2017-314
Manuscript under review for journal Atmos. Meas. Tech.
Discussion started: 4 October 2017

Atmospheric Measurement Techniques Discussions

Table 1 – Posterior errors estimated from the sample standard deviations of the retrieval output. In each case, σ refers to the full sample standard deviation and σ (filtered) refers to the sample standard deviation excluding those with the 10 % highest values of χ^2. The bottom row shows the mean of the standard deviations entered in each row.

	τ		ctP (hPa)		dP (hPa)	
True τ	σ	σ (filtered)	σ	σ (filtered)	σ	σ (filtered)
5	0.22	0.22	6.5	6.3	5.3	5.3
10	0.27	0.25	13.7	2.3	22.0	2.5
15	0.46	0.45	1.8	1.8	1.0	1.0
20	0.15	0.15	1.3	1.3	0.8	0.8
25	0.13	0.13	1.4	1.3	0.9	1.0
30	0.32	0.32	1.5	1.4	1.2	1.1
35	7.52	1.95	19.5	2.9	11.3	3.1
40	15.27	0.49	26.7	2.3	26.4	0.9
Average	6.02	0.75	12.9	2.9	12.9	2.5